



The influence of Mn doping on the leakage current mechanisms and resistance degradation behavior in lead zirconate titanate films

Betul Akkopru-Akgun^{a,b,*}, Thorsten J.M. Bayer^d, Kosuke Tsuji^{a,b}, Clive A. Randall^{a,b}, Michael T. Lanagan^{a,c}, Susan Trolier-McKinstry^{a,b}

^a Center for Dielectrics and Piezoelectrics, Materials Research Institute, The Pennsylvania State University, University Park, PA 16802, United States

^b Department of Materials Science and Engineering, The Pennsylvania State University, University Park, PA 16802, United States

^c Department of Engineering Science and Mechanics, The Pennsylvania State University, University Park, PA 16802, United States

^d TDK Electronics GmbH & Co OG, Deutschlandsberg, Österreich, 8530, Austria



ARTICLE INFO

Article history:

Received 12 August 2020

Revised 29 December 2020

Accepted 18 January 2021

Available online 1 February 2021

Keywords:

Electrical degradation

PZT, Thin films

Defect chemistry

Electrical conduction

ABSTRACT

The electrical reliability of lead zirconate titanate (PZT) films was improved by incorporating Mn; the time dependent dielectric breakdown lifetimes and the associated activation energy both remarkably increased with Mn concentration. The correlation between the defect chemistry and the resistance degradation was studied to understand the physical mechanism(s) responsible for enhanced electrical reliability. At lower electric fields, Poole-Frenkel emission was responsible for the leakage current. Beyond a threshold electric field, Schottky emission controlled the leakage. After electrical degradation of a 2 mol.% Mn doped PZT film, no significant change in potential barrier height for injecting electrons from the cathode into the anode was observed. This suggests that the degradation is mostly controlled by Poole-Frenkel conduction via some combination of hole migration between lead vacancies, small polaron hopping between Mn sites, and hole hopping between Pb^{2+} and Pb^{3+} . No variation in the valence state of Ti near the cathode was observed in degraded Mn doped PZT films, implying that multivalent Mn provides trap sites for electrons and holes; free electron generation due to compensation of oxygen vacancies at the cathode and free hole formation at the anode region might be suppressed by the valence changes from Mn^{3+} to Mn^{2+} and Mn^{2+} to Mn^{3+} respectively.

© 2021 Acta Materialia Inc. Published by Elsevier Ltd. All rights reserved.

1. Introduction

The performance and electrical reliability of lead zirconate titanate (PZT) piezoelectric films used in microelectromechanical systems (MEMS), [1–8] are typically controlled by point defects. Acceptor type impurities like $Fe^{2+/3+}$, $Mn^{2+/3+}$, Mg^{2+} have lower valence than the B-site cations (Ti^{4+} , Zr^{4+}) they replace. Charge compensation is achieved by generating oxygen vacancies and/or holes in the system; [9] in some cases, these point defects associate to create defect dipoles such as $(A''_{Ti} - V_O)^x$, $(A'_{Ti} - V_O)'$ in Kroger-Vink notation. For multivalent acceptor ions like $Mn^{2+/3+/4+}$ or $Fe^{2+/3+/4+}$, the valence state varies with the annealing atmosphere [10]. Hayashi et al. showed that processing of Mn doped $PbTiO_3$ in oxidizing atmospheres results in isovalent doping (Mn^{4+} substituting for Ti^{4+}) and low oxygen vacancy concentrations, whereas annealing under a reducing atmosphere leads to aliovalent doping ($Mn^{2+/3+}$ on Ti^{4+}) and higher oxygen vacancy concen-

trations [11,12]. Thus, the hole or/and oxygen vacancy concentrations can be engineered to govern the electrical properties of PZT films.

In contrast to acceptors, donor impurities like Nd^{3+} or La^{3+} on the A-site (Pb^{2+}) or Nb^{5+} on the B-site (Ti^{4+} , Zr^{4+}) are either ionically and/or electronically compensated via doubly ionized lead vacancies and electrons, respectively. Addition of donor ions into PZT suppresses the number of oxygen vacancies below the intrinsic level.

Table 1 gives activation energy data for ionic and/or electronic conduction and associated degradation mechanisms observed in different lead-based perovskites [13–25]. Given that the defect chemistry of bulk ceramics and crystals is likely to differ from that of thin films, it is interesting to consider the impact of this on time-dependent degradation. There are a number of important differences that influence the defect chemistry and the charge transport mechanisms responsible for DC resistance degradation in thin films. Three of the critical disparities are (1) the processing of thin films is typically conducted under conditions where the sample is not in thermodynamic equilibrium; this can result in higher point

* Corresponding author.

E-mail address: bu134@psu.edu (B. Akkopru-Akgun).

Table 1

Reported activation energies in PZT and other lead-based perovskites. HALT = highly accelerated lifetime testing, DLTS = deep level transient spectroscopy, ToF-SIMS = time of flight secondary ion mass spectroscopy, EPR = electron paramagnetic resonance.

Composition	Method	E_a (eV)	Mechanism	Reference
(Mg, Nb) co-doped PZT bulk (Mn, Nb) co-doped PZT bulk	Impedance measurement	1.05–1.25 eV 1.48 eV	Ionic conductivity by $V_O^-V_{Pb}''$ diffusion	(Ref. 13)
PZT film	HALT	0.78 eV	Ionic migration of V_O^-	(Ref. 14)
Pb(Zr _{0.54} Ti _{0.46})O ₃ film	DLTS	0.27 eV	Hopping between Pb ²⁺ and Pb ³⁺	(Ref. 15)
PbZr _{0.65} Ti _{0.35} O ₃ film	ToF-SIMS-O ¹⁸ tracer diffusion	2.7 eV 0.6 eV	Near-surface oxygen tracer diffusivity "Bulk" diffusivity	(Ref. 16)
PZT film PNZT film PLZT film	HALT	0.6–1.2 eV	Hole trapping by V_{Pb}'' or acceptor impurities	(Ref. 17)
PbZr _{1-x} Ti _x O ₃ bulk	EPR	0.26 eV 1 eV	Hopping between Pb ²⁺ and Pb ³⁺ Electron trapping via Ti ⁴⁺ sites	(Ref. 18)
Pb _{1.01} Ti _{1.00} O _x films Pb _{1.00} Ti _{1.00} O _x films	DLTS	0.25–0.27 eV 0.46–0.50 eV 0.93–1.01 eV	Hopping between Pb ²⁺ and Pb ³⁺ Ionization of lead vacancies	(Ref. 19)
Pb _{1.01} Ti _{1.00} O _x films	Impedance measurement	0.99–1.21 eV	Ionization of oxygen vacancies	(Ref. 20)
(Pb _{1-x} La _x)(Zr _{0.90} Ti _{0.10}) _{1-x/4} O ₃	HALT	0.87 eV	Migration of oxygen vacancies	(Ref. 21)
Nd doped Pb(Zr _{0.52} Ti _{0.48})O ₃ films	I-V	0.5–0.6 eV	Ionization energy of Ti ⁴⁺ to Ti ³⁺	(Ref. 22)
Pb(Zr,Ti)O ₃	Impedance measurement	0.98–1.28eV	V_O^- trapping level for electrons	(Ref. 23)
(Pb _{1-x} Ba _x)(Zr _{0.95} Ti _{0.05})O ₃	Impedance measurement	0.54 eV	V_O^- Singly ionized oxygen vacancies	(Ref. 24)
Mn doped PMN-PT single crystal	HALT, Impedance measurement, TSDC	0.6 eV 1.4 eV 1.1 eV	Ionic migration of V_O^- ; Hole migration between V_{Pb}'' localized Ti ³⁺ Electron hopping from	(Ref. 25)

defect concentrations and metastable structures, (2) interfaces have a much stronger influence on point defect chemistry in films than in bulk materials; the equilibrium concentration of a point defect is strongly dependent on formation energy of defects at the interface, and (3) as feature size is scaled down, the diffusion length over which defects must move to induce degradation becomes shorter. In particular, the defect chemistry in PZT films is very difficult to control precisely due to unknown cation stoichiometry resulting from evaporation of PbO upon annealing.

As shown in Table 1, a wide variation in activation energy for a failure under a DC bias field was observed depending on the type and concentration of impurity and the film stoichiometry [13–25]. In general, fixed-valence acceptor doped PZT films exhibit lower lifetime than their donor doped counterparts since the addition of acceptor ions in the perovskite lattice leads to formation of oxygen vacancies; [26] it is believed that the field driven migration of oxygen plays a critical role in DC resistance degradation [27,28]. It was shown in BaTiO₃ and SrTiO₃ that resistance degradation can be associated with migration of oxygen vacancies and subsequent buildup near the cathode and depletion near the anode [27,29]. Surprisingly, Pb based perovskites with redox-active acceptor ions exhibit longer lifetimes and lower electrical degradation rates [25]. Enhanced lifetime via introduction of Mn has been reported by Yoon et al. for BaTiO₃ ceramics, [30,31] Mori et al. for PZT films, [32] and Yan et al. for PMN-PT ceramics [33]. Two different mechanisms were proposed to explain the improvement in lifetime via addition of Mn into PZT films; (1) Jahn-Teller distortion of Mn³⁺ oxygen polyhedra may retard the dissociation of Mn_{Ti}' - V_O' defect dipoles and subsequent migration of oxygen vacancies upon electrical degradation, [31] (2) e' - h' trapping; electrons accumulated near the cathode and hole formation in anodic region can be suppressed by introducing Mn into PZT films [25]. Although it is well understood that Mn doping plays a critical role in defect chemistry and resistance degradation, the exact mechanism has not yet been clarified.

In this work, the influence of Mn in altering the defect structure and associated charge transport mechanisms has been studied in PZT films; it is shown that multivalent acceptor ions can be used to engineer defect types and concentrations in the perovskite lattice. The nature and concentrations of point defects, their migration under electric field, and electronic carrier distributions were explored by in-situ impedance, DLTS (Deep Level Transient Spectroscopy) and TSDC (Thermally Stimulated Depolarization Current). The change in interfacial defect chemistry was monitored via Electron Energy Loss Spectroscopy. The dominant conduction mechanism leading to resistance degradation in Mn doped PZT films was explored by I-V measurements. The lifetimes of PZT films with different Mn concentrations were assessed using Highly Accelerated Lifetime Testing (HALT), from which activation energies and voltage acceleration factors were extracted. A physical model for the failure process was developed to facilitate design of electrically reliable PiezoMEMS.

2. Experimental procedure

Mn-doped lead zirconate titanate (PZT) thin films of 400±15 nm thickness at the morphotropic phase boundary (MPB) composition with dopant concentrations varying from 0.5 to 4 mol% were prepared on Pt/Ti/SiO₂/Si substrates (Nova Electronic Materials, Flower Mound, TX) by chemical solution deposition. 10 mol% Pb excess was added to precursor solutions to compensate lead loss during heat treatment. The final film composition was estimated as Pb_{(1-1/2x)}}Zr_{0.52(1-x)}}Ti_{0.48(1-x)}}Mn_xO₃, where x = 0.005–0.04. The details of the preparation of the PZT films were described elsewhere [34].

For electrical measurements, an array of ~100 nm thick sputtered Pt top electrodes with diameters of 200 μm, 400 μm, 600 μm, and 1 mm were patterned on PZT films by photolithography and lift off processing. Prior to electrical measurements, PZT films were post-annealed at 600°C for 1 min using rapid thermal annealing (RTA) with a ramp rate of 50°C/sec in an O₂ flow.

An FEI TITAN transmission electron microscope (TEM, FEI, G2) was utilized with an accelerating voltage of 200 kV to investigate the interface structure and composition of the PZT films. Variation in oxidation state of Ti across the electrically degraded PZT film was examined via electron energy-loss spectroscopy (EELS) using an operating voltage of 80 kV, 2.5 mm aperture and an energy dispersion of 0.01 eV/pixel.

Leakage current measurements of PZT films were conducted on PZT films using a Hewlett Packard 4140 pA meter. The waiting time at each voltage increment was set to 60 seconds to stabilize the current prior to collecting the data.

Thermally stimulated depolarization current, TSDC, measurements were conducted using a HP 4140b pA meter between 25 and 300°C. First, the PZT film was poled at 180°C under an electric field of 350 kV/cm for 3, 6, and 12 h to align defect dipoles, trapped charges, and space charges. The PZT film was then cooled down to room temperature under an electric field to freeze the polarized defects. Finally, the sample was heated at zero bias voltage using a constant heating rate and the depolarization current was monitored with a pA meter.

Highly accelerated lifetime testing, HALT, was conducted on Mn doped PZT films at temperatures from 150 - 200°C with DC electric fields of 250 - 450 kV/cm to explore the median time to failure and lifetime-determining charge transport mechanisms responsible for electrical degradation in PZT films. First, 1 cm² PZT thin film samples were attached to a DIP package using silver paste. Then, gold wire bonding was utilized to connect the top Pt electrodes to the contact pads of the DIP. The leakage current increase upon electrical degradation was simultaneously recorded for eight different 400 μm diameter top platinum electrodes. The Prokopowicz and Vaskas empirical model was employed to describe the electrical reliability of PZT films at accelerated test conditions [35].

$$\frac{t_1}{t_2} = \left(\frac{V_2}{V_1}\right)^n \exp\left[\frac{E_a}{k} \left(\frac{1}{T_1} - \frac{1}{T_2}\right)\right] \quad (1)$$

where t is the median time to failure ($t_{0.5}$), k is Boltzmann's constant, V is voltage, T is temperature, and E_a , is activation energy. $t_{0.5}$ was calculated using Weibull analysis.

To assess the presence of shallow trap sites, Charge based Deep Level Transient Spectroscopy (Q-DLTS) measurements were conducted using a charging voltage of 4V and 100 μs duration time. The magnitude of the Q-DLTS signal is $\Delta Q = Q(t_2) - Q(t_1)$, where t_1 and t_2 are discharging durations. The ΔQ signal was recorded as a function of temperature and electric field for a constant rate window $\tau_m = (t_2 - t_1) - \ln(t_2/t_1)$. The charge released within Δt is described based on Eq. (2) [36,37].

$$Q(t) = Q_0[\exp(-e_p t_1) - \exp(-e_p t_2)] \quad (2)$$

where $Q_0 = \int_0^\infty Q_0(t)dt$. For hole traps, $e_p = \sigma v_{th} N_C \exp(-E_a/kT)$ is the hole emission rate, $v_{th} = \sqrt{\frac{3kT}{m_e^*}}$ = electron thermal velocity, $N_C = 2\left(\frac{3kT}{m_e^*}\right)^{3/2}$ = effective density of states in the conduction band, m_e^* is the effective mass of the hole or electron and σ is the capture cross section of the trap states [36].

In-situ impedance analysis was performed using an Agilent E4980A Precision LCR Meter (Santa Rosa, CA). First, the impedance spectrum of an undegraded (pristine state) PZT film was taken using an AC amplitude of 100 mV at frequencies from 2MHz to 20 Hz. A DC voltage of 40 kV/cm was then applied at 320°C and impedance measurements were acquired until the degradation

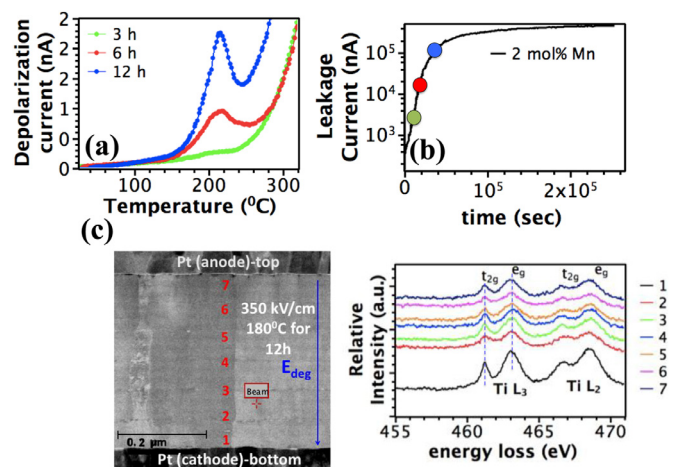


Fig. 1. Change in (a) leakage current with time, (b) TSDC spectra of 2% Mn doped PZT films upon degradation at 180°C under an electric field of 350 kV/cm for 3, 6, or 12 h, (c) Electron energy loss spectra of electrically degraded 2 mol% Mn doped PZT film as a function of distance from the cathode. The numbers shown in red represent the regions where EELS data were taken; 1 and 7 are areas near the bottom Pt/PZT and the top Pt/PZT interfaces, respectively and 2 to 6 represent areas in the individually deposited PZT layers.

process was completed. The DC voltage was removed to investigate the change in impedance during the recovery process, as shown in Figure S.1. A Solartron Analytical Modulab XM (Oak Ridge, USA) was used to investigate the temperature dependence of modulus spectra at frequencies from 1 MHz to 1 mHz.

3. Results and discussion

Figure S.2 shows the time-dependence leakage current for Mn doped PZT films under an electric field of 350 kV/cm at 180°C. Weibull analysis was performed to obtain the distribution of degradation rates and $t_{0.5}$ (Figure S.2b). The $t_{0.5}$ increases remarkably with Mn concentration in PZT films from 1.47 ± 0.2 , 3.9 ± 0.4 , 7.9 ± 0.9 , and 21.4 ± 0.8 h for 0.5, 1, 2, and 4 mol% Mn doped PZT films, respectively (Table S.1). The activation energy for electrical degradation increases with Mn concentration in PZT films; activation energies of 0.76 ± 0.06 , 0.97 ± 0.05 , 1.15 ± 0.04 , and 1.33 ± 0.06 eV were found for 0.5, 1, 2, and 4 mol% Mn doped PZT films, respectively. (Figure S.3, Table S.3). A voltage acceleration factor of 4.8 ± 0.24 and 5.6 ± 0.3 was found for 1 and 2 mol% Mn doped PZT films, which is similar to the values reported in the literature [14,17,38]. Degradation in perovskite-type ceramics is often due to the field driven migration of oxygen vacancies (exacerbated at elevated temperatures) and subsequent accumulation of oxygen vacancies near the cathode [27]. Thus, it is unexpected to observe higher lifetimes in PZT films with higher Mn concentrations, as Mn increases the oxygen vacancy concentration, as shown via the electroneutrality condition in Eq. (3).

$$2[Mn''_{Ti}] + [Mn'_{Ti}] + 2[V''_{Pb}] + [e'] = 2[V'_O] + [h'] \quad (3)$$

To assess the presence of mobile or/and trapped oxygen vacancies, Thermally Stimulated Depolarization Current Measurements (TSDC) were performed on degraded Mn-doped PZT films (Fig. 1a,b). Only one depolarization current peak was observed around 200°C. The T_p dependence of T_{max} was studied to explore the physical origin of this peak; the corresponding activation energy was calculated using the initial rise method described elsewhere [39,40]. It was found that the peak is due to ionic migration of oxygen vacancies with an activation energy of 0.6 eV [40]. Thus, the dissociation of defect dipoles, $(Mn''_{Ti} - V'_O)^x$, $(Mn'_{Ti} - V'_O)^y$, $(V''_{Pb} - V'_O)^x$, along with the migration of V'_O upon electri-

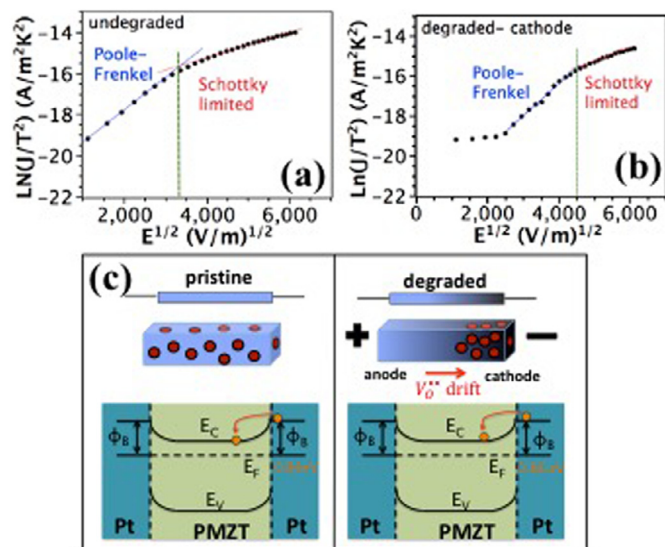


Fig. 2. Fitting of the leakage current-voltage results for (a) undegraded and (b) degraded 2 mol% Mn doped PZT thin films at 180°C under an electric field of 350 kV/cm for 12 h. (c) Schematic picture of oxygen vacancy migration and subsequent change in potential barrier height for injecting electrons

cal degradation leads to growth of an ionic space charge peak. The concentration of oxygen vacancies increased from 3×10^{19} to 5×10^{19} , 1×10^{20} , and $2 \times 10^{20}/\text{cm}^3$ with increasing Mn concentration from 0.5 to 1, 2, and 4 mol%, respectively, [40] which confirms that the ionic conductivity due to long-range migration of oxygen vacancies was not eliminated due to Jahn-Teller distortions.

Ionic migration and subsequent accumulation of $V_O^{\bullet\bullet}$ under DC field changes the local defect chemistry through the PZT films; electrons are created in the cathodic region, and holes are generated in the anodic region by accumulation and depletion of $V_O^{\bullet\bullet}$, respectively. This results in a substantial increase in leakage current and lowering of the barrier for electron injection from the cathode into the film. The compensating electrons can be trapped at Ti^{4+} to create Ti^{3+} , [18] as was reported in Nb-doped PZT [41].

Fig. 1c depicts a series of Ti-L edges in 2 mol% Mn doped PZT film as a function of distance from the cathode. Prior to EELS analysis, the film was severely degraded under an electric field of 350 kV/cm for 12 h. No obvious chemical shift was found from EELS spectra taken from cathodic region to anodic region, indicating that oxidation state of Ti remained unchanged in degraded Mn doped PZT films.

Moreover, TSDC results of degraded Mn doped PZT films did not show a depolarization current peak arising from relaxation of trapped electrons from Ti^{4+} . This suggests that free electron generation due to compensation of $V_O^{\bullet\bullet}$ at the cathode and free hole formation at the anode region might be suppressed by the valence changes from Mn^{3+} to Mn^{2+} and Mn^{2+} to Mn^{3+} respectively. The compensated electrons near the cathode region are more likely trapped on the manganese sites rather than Ti^{4+} ions, since $\text{Ti}_{\text{Ti}}^{\times}$ is less reducible than $\text{Mn}_{\text{Ti}}^{\times}$ and $\text{Mn}_{\text{Ti}}^{\bullet}$ ions [42].

To further explore the change in charge transport mechanism through chemical modification of PZT films, the conduction mechanism of pristine and degraded Mn doped PZT films was investigated. Fig. 2 shows the fit of the I-V results to the equations for distinct electronic conduction mechanisms. In the pristine state, the conduction mechanism below 145 kV/cm is dominated by Poole-Frenkel emission, whereas the high electric field range is controlled by Schottky emission. The Schottky barrier height was extracted from Schottky plots in the field range of 180-400

kV/cm and calculated to be 1.17 ± 0.04 , 1.06 ± 0.05 , 0.84 ± 0.03 , and 0.72 ± 0.04 eV for 0.5, 1, 2, and 4 mol% Mn doped PZT films (Table S.4). The experimental value is significantly lower than the theoretical value ($\phi_B = \phi_M - \chi_{\text{PZT}} = 1.8$ eV), calculated based on the metal work function (5.3 eV) and the electron affinity of the PZT (3.5 eV), suggesting that the barrier height at the metal-PZT interface is strongly influenced by interface/surface states such as oxygen vacancies and/or impurity levels. Scott et al. [43,44] reported that oxidation and reduction of the PZT/Pt interface leads to changes in E_f of more than 1 eV. [45]. Reduction of the oxide surface creates a high concentration of defects, most likely $V_O^{\bullet\bullet}$, at the PZT/Pt interface that pin the Fermi level. This lowers the potential barrier height and enhances the probability of electron injection from the cathode to the PZT. In the same way, the barrier height decreases from 1.17 eV to 0.72 eV as the Mn concentration increased from 0.5 to 4 mol% due to modification of Schottky barrier through Fermi level pinning.

After degrading 2 mol% Mn doped PZT films under an electric field of 350 kV/cm at 180°C for 12 h, (1) the width of Poole-Frenkel regime increases, accompanied by a shrinkage in the field range for the Schottky regime; the transition electric field from Poole-Frenkel conduction to Schottky emission shifted from 145 to 182 kV/cm after degradation and (2) insignificant variation in potential barrier height for injecting electrons from cathode into PZT was observed after degradation; Schottky barriers of 0.84 ± 0.05 and 0.86 ± 0.07 eV were found in pristine and degraded states, respectively. Thus, unlike observations on Nb-doped PZT films, the Schottky barrier height in Mn-doped PZT does not change on degradation.

The current density, J , at a Schottky contact can be described by:

$$J = J_0 \exp\left(\frac{qE}{nkT}\right) \left[1 - \exp\left(\frac{qV}{kT}\right)\right] \quad (4)$$

where J_0 is the reverse saturation current, and k and n are Boltzmann's constant and the ideality factor, respectively. J_0 , the reverse saturation current is represented by: [46,47]

$$J_0 = A^* T^2 \exp\left(-q \frac{q\phi_B}{kT}\right) \exp\left[\frac{q\sqrt{qE/4\pi\epsilon_0\epsilon_r w}}{kT}\right] \quad (5)$$

where A^* , ϕ_B , ϵ_0 , ϵ_r , and w are the Richardson's constant, the potential barrier height, vacuum permittivity, dielectric constant, and depletion layer thickness, respectively. In Eq. (4), it is assumed that E , which determines the barrier lowering, is uniform throughout the PZT film, which necessitates that the film is fully depleted. However, $E \neq V/d$ in the case of partial depletion. Accumulation of $V_O^{\bullet\bullet}$ at the negatively biased Schottky interface leads to a variation in the maximum field strength in the barrier, E_m ; the high resulting dopant concentration allows the applied electric field to be gradually diminished across a depletion layer near the cathode. In this case, E_m is described by: [47,48]

$$E_m = \sqrt{\frac{2qN_D}{\epsilon_s} \left(V - V_{bi} - \frac{kT}{q}\right)} \quad (6)$$

where q , N_D , ϵ_0 , ϵ_{DC} , V , V_{bi} , k , T are electric charge, vacuum permittivity, dielectric constant, applied voltage, built-in potential, Boltzmann's constant, and temperature, respectively. The maximum field strength in the barrier, E_m , is directly proportional to $\exp(q\Delta\phi_B/kT)$, where $\Delta\phi_B$ is the lowering of the barrier due to the field. Upon degradation of 2 mol% Mn doped PZT films, $V_O^{\bullet\bullet}$ accumulate near the cathode. This leads to a decrease in the depletion layer width, $w = \sqrt{2\epsilon_0\epsilon_r(V_a - V_b)/qN_d}$ [47,49]. This exponentially increases the leakage current, accompanied by Schottky barrier lowering and eventually electrical breakdown of the film.

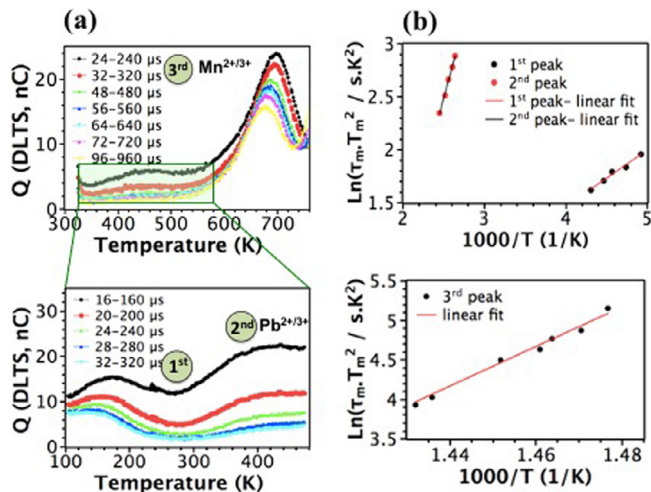


Fig. 3. (a) Q-DLTS of 2 mol% Mn doped PZT films from 300 to 750 K. The DLTS signal was measured at seven different rate windows (see legends for t_1 and t_2) to resolve emission from different traps, (b) Arrhenius plot of the DLTS signal

However, in this study, no change in Schottky barrier height was observed upon electrical degradation. This could be attributed to suppression of the electric field in the depletion layer via trapping of electronic charges by Mn near the interface, which screens the space charge due to accumulation of $V_{O\bullet}$. This trapping creates a double electrical layer consisting of the negatively charged interfacial layer due to trapped electrons via Mn sites and positively charged space charge region as a result of accumulation of $V_{O\bullet}$. When the carrier density is very high, the total space charge region near the interface becomes neutral by offsetting the positive space charge with the negative surface charge. Under this circumstance, barrier lowering, ϕ_{Δ_B} is limited by the suppressed electrical field due to the presence of trapped charges at Mn sites. Moreover, the distribution of trapped charges associated with Mn sites extends over long distances because the Mn concentration is modest. This could also reduce the electric field in the depletion region, which in turn decreases barrier lowering and suppresses leakage current increase upon electrical degradation.

To assess the different trap levels that contributes to Poole-Frenkel emission in Mn doped PZT films, Q-DLTS measurements and impedance analysis were conducted. Fig. 3 depicts the DLTS signals of 2 mol% Mn doped PZT films from 100–650K. The DLTS signals reveal three distinct peaks, referred to as traps 1, 2, and 3. The electron emission rate is given by:

$$e_n = \tau_n^{-1} = \sigma_n \gamma_n T^2 \exp\left(-\frac{E_T}{kT}\right) \quad (7)$$

where σ_n is the capture cross section, γ_n is a constant, τ_n is the emission time constant, k is Boltzmann's constant, and E_T is the trap activation energy. The maximum temperature points for DLTS peaks are plotted on an Arrhenius plot for different rate windows (Fig. 3b). The activation energy and capture cross section of defect states were extracted from the slope and intercept of the Arrhenius plot, respectively; the results are shown in Table S.3. The first DLTS peak with the small activation energy of 0.05 eV is most likely associated with hopping conduction. The second trap level with an activation energy of 0.26 eV was attributed by Smyth et al. to hole hopping between Pb^{2+} and Pb^{3+} sites [18]. The third DLTS peak with an activation energy of 1.9 eV is associated with Mn^{2+}/Mn^{3+} impurity levels in the energy band diagram of PZT [50].

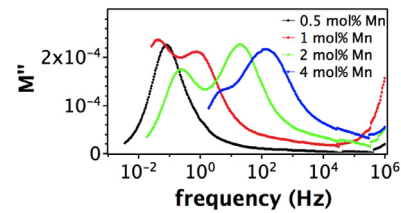


Fig. 4. Modulus spectra at different frequencies for 0.5, 1, 2, and 4 mol% Mn doped PZT films in pristine state at 240°C.

The TSDC results demonstrate that the concentration of accumulated oxygen vacancies near the cathode upon degradation is $1 \times 10^{20}/cm^3$. In principle, a high concentration of compensating electrons $n \sim 2[V_{O\bullet}] = 2 \times 10^{20}/cm^3$ should exist near the cathode. These electrons could be trapped by Mn; each Mn ion can trap not more than two electrons. Since the Mn ions are widely distributed within the film due to their low concentrations, the trapped electrons at Mn sites are also spread out, which shifts the center of charge from the cathode region towards the bulk of the film. This prevents accumulation of electrons at the cathode/PZT film interface, which decreases barrier lowering and leakage current increase upon degradation, consistent with the experimental observations.

Figure S.4. exhibits the imaginary part of the electric modulus and impedance of a pristine 2 mol% Mn doped PZT film measured at 320°C; $M''(f)$ indicates the volume fraction with similar conductivity [51–54]. The conductivity σ of the film is related to the relaxation frequency f_r through the equation:

$$\sigma = 2\pi f_r \epsilon_0 \epsilon_r \quad (10)$$

where ϵ_0 and ϵ_r are the vacuum and relative permittivities, respectively.

As shown in Figure S.4., the imaginary part of the electric modulus for the 2 mol% Mn doped PZT film consists of two peaks, indicating the presence of two regions with different conductivities. This inhomogeneous conductivity might arise from (1) the presence of regions with distinct charge transport mechanisms and/or (2) non-uniform distribution of oxygen vacancies and other defects in the sample.

Figure S.5 shows the imaginary part of the electric modulus for 2 mol% Mn doped PZT films with different thicknesses. The magnitude of the modulus peak, which is inversely proportional to the permittivity of the PZT film at the relaxation frequency, is independent of thickness for films from 350–1200 nm. This indicates that the modulus peak is associated with bulk charge transport rather than an interface-controlled mechanism.

The magnitude and relaxation frequencies of the imaginary part of the electric modulus peaks depend on the Mn concentration as shown in Fig. 4. For the 0.5 mol% Mn doped PZT film, the modulus spectrum consists of only one peak at 0.04 Hz, representing a homogeneous conductivity profile with a comparably low conductivity. As the Mn concentration increases to 1 mol% in PZT films, a second modulus peak appears at 20 Hz and the intensity of this peak gradually increased while the first peak is progressively suppressed with further increase in Mn concentration. In addition, the first peak shifts to higher frequencies, suggesting that the conductivity of the Mn doped PZT film increases with increased Mn concentration.

Fig. 5 shows the temperature dependence of the modulus peak. The activation energies extracted for 0.5–4 mol% Mn doped PZT films are shown in Fig. 5e. The activation energy for the low frequency modulus peak was found to be 1.39 ± 0.05 eV, which is associated with hole migration between V_{Pb}'' ; this peak is largely independent of the Mn concentration [55]. The activation energy

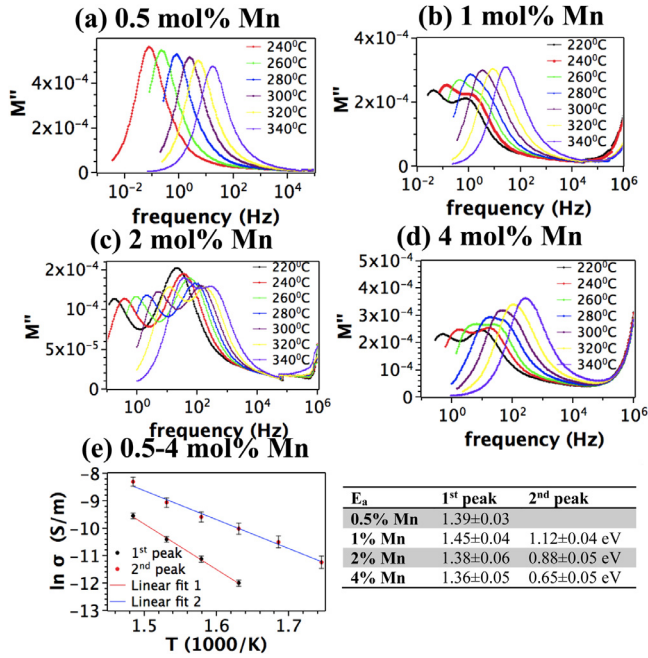


Fig. 5. Temperature dependence of modulus in (a) 0.5, (b) 1, (c) 2, and (d) 4 mol% Mn doped PZT films, (e) Arrhenius plots for conductivity in 2 mol% Mn doped PZT films and corresponding activation energies for low and high frequency peaks

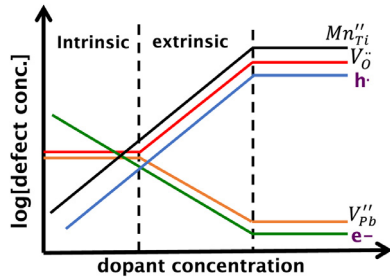


Fig. 6. Schematic representation of defect concentrations as a function of Mn dopant level in PZT films

of the higher frequency modulus peak, on the other hand, gradually decreases from 1.12 to 0.65 eV with increasing Mn concentration. This suggests a gradual change in charge transport mechanism from hole migration between V_{Pb}^{2-} to hole hopping and/or trapping between Mn ions. Indeed, as the Mn concentration increases in the PZT films, the hole concentration rises and $Mn^{2+/3+}$ ions start to serve as hole trapping sites (Fig. 6). Consequently, the contribution of V_{Pb}^{2-} to the total electronic conduction declines with addition of Mn.

The temperature dependent conductivity of 1–4 mol% Mn doped PZT films were fitted using the small polaron hopping (SPH) model (Fig. 7) proposed by Emin and Holstein, [56] which can be expressed by: [57]

$$\sigma = ne\mu = \frac{\sigma_0}{T} \exp\left(\frac{-E_a}{k_B T}\right), \quad \sigma_0 = \frac{gNc(1-c)e^2 r^2 \nu}{k_B}, \quad r = \left(\frac{1}{N}\right)^{1/3} \quad (11)$$

where σ_0 is the pre-exponential factor, c is the fraction of sites occupied by polarons, n is the number of charge carriers [$n = N \cdot c \cdot (1-c)$], N is the density of conducting sites, r is the site-to-site hopping distance, ν is the characteristic vibrational frequency, and E_a is the hopping activation energy. As shown in Fig. 7, the fit is good, suggesting that the electrical transport in Mn doped PZT films is dominated by phonon-assisted hole hopping between Mn sites.

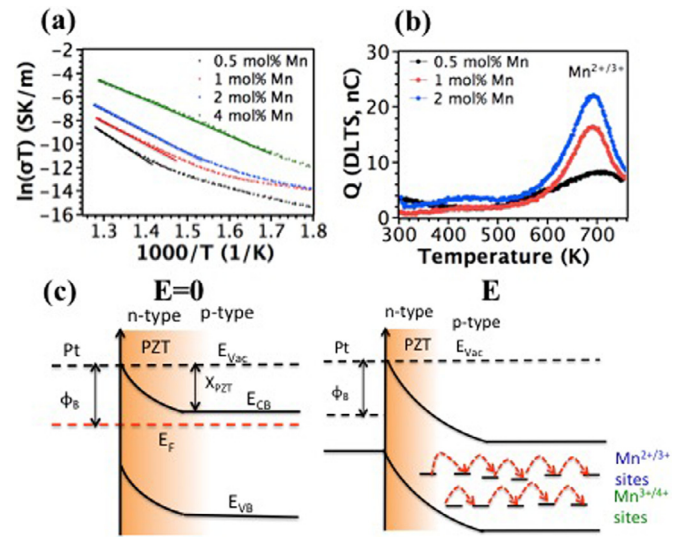


Fig. 7. (a) Temperature dependence of conductivity in 0.5, 1, 2, and 4 mol% Mn doped PZT films, (b) DLTS spectra of 0.5, 1, and 2 mol% Mn doped PZT films, (c) Schematic representation of Mn impurity sites in PZT energy band diagram without and with an applied electric field.

The density of conduction sites, which is directly proportional to the Q-DLTS signal, increases gradually with the Mn concentration (Fig. 7b). Thus, the hopping distance, which scales as $r = (N)^{-1/3}$, is lower for 2 mol% Mn doped PZT films. Since ν should vary only slightly with Mn doping, the increase in conductivity with Mn doping is due to N and r . The drop in hopping distance with Mn doping decreases the pre-exponential factor, σ_0 and the activation energy, E_a . These two factors enhance the small polaron hopping conduction between $Mn^{2+/3+}$ and $Mn^{3+/4+}$ sites (Fig. 7c) and result in a significant increase in the electronic conductivity.

The contribution of electronic conduction to the DC resistance degradation of Mn doped PZT films was investigated using in-situ impedance spectroscopy, as shown in Fig. 8. Only some frequency sweeps are shown for clarity. The pristine state of 0.5 mol% Mn doped PZT is characterized by only one maxima at 28 Hz (hence a homogenous conductivity profile) whereas two distinct maxima at 47.6 and 528 Hz were observed for 4 mol% Mn doped PZT films, indicating the existence of regions with distinct conductivities. A DC voltage of 40 kV/cm was applied at 320°C and impedance measurements were acquired continuously during degradation. Both peaks shift to higher frequencies as degradation progresses in 4 mol% Mn doped PZT films; the magnitude of shift with degradation time is more noticeable in the first modulus peak. The bulk conductivity increases three orders of magnitude throughout the film on degradation. After 912s, the first peak started to merge with the second peak and the combined peak narrowed with increasing degradation time. This suggests that the conductivity profile of 4 mol% Mn doped PZT films became more homogenous as degradation progressed.

Similar to 4 mol% Mn doped PZT films, the single modulus peak shifted through higher frequencies with degradation time in 0.5 mol% Mn doped PZT films, indicating a gradual increase in the conductivity of the film. For both 0.5 and 4 mol% Mn doped PZT films, the modulus peak stabilized after 22054 s of degradation.

After degradation, the DC voltage was turned off. During recovery, the modulus peak decreases in relaxation frequency and increases in the magnitude. However, the modulus peak did not reach its original undegraded position within a recovery time of 77400 s at 320°C for 0.5 mol% Mn doped PZT films. Similarly, the admittance of the recovered sample didn't reach that of the pris-

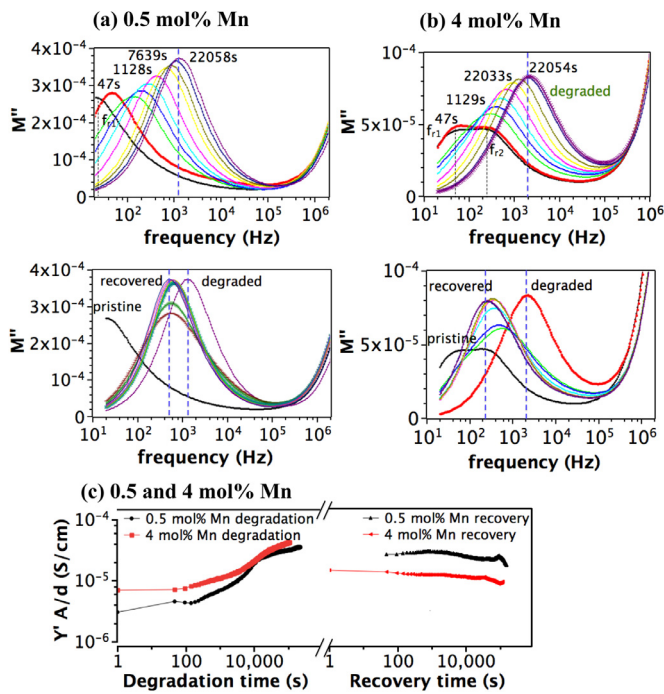


Fig. 8. Imaginary modulus spectra of (a) 0.5 and (b) 4 mol% Mn doped PZT films during electrical degradation and recovery at 320°C, (c) change in admittance of 0.5 and 4 mol% Mn doped PZT films during degradation and recovery.

tine state, as indicated in Fig. 8c. This indicates that the conductivity of the recovered state exceeds that of the pristine sample. This suggests that a slow process like the drift of V_O^{\bullet} controls both degradation and recovery in 0.5 mol% Mn doped PZT films. For 4 mol% Mn doped PZT films, on the other hand, the recovery rate is much faster; an order of magnitude decrease in the conductivity was observed within 40s of recovery. This strongly suggests that the conductivity increase upon degradation is dominated by electronic conduction rather than ionic migration of defects. It is plausible that higher Mn concentrations increase small polaron hopping conduction, leading to a dramatic increase in the contribution of electronic conduction ($\frac{\sigma_{\text{electronic}}}{\sigma_{\text{ionic}}}$) to the conductivity.

4. Conclusions

0.5, 1, 2, and 4 mol% Mn-doped (PMZT) lead zirconate titanate films were grown on platinumized Si substrates by chemical solution deposition. In the pristine state, the conduction mechanism below 145 kV/cm is dominated by Poole-Frenkel emission, whereas, at higher electric fields, the conduction is controlled by Schottky emission. The potential barrier height was 1.17 ± 0.04 , 1.06 ± 0.05 , 0.84 ± 0.03 , and 0.72 ± 0.04 eV for 0.5, 1, 2, and 4 mol% Mn doped PZT films. The variation in Schottky barrier height with Mn concentration is attributed to Fermi level pinning by interface states, mostly oxygen vacancies.

After degrading Mn doped PZT films under an electric field of 350 kV/cm at 180°C for 12 h, (1) the width of Poole-Frenkel regime increases, accompanied by a shrinkage in the field range for the Schottky regime; the transition electric field from Poole Frenkel conduction to Schottky emission shifted from 145 to 182 kV/cm after degradation and (2) trivial alteration in potential barrier height for injecting electrons from cathode into PZT was observed after degradation; Schottky barriers of 0.84 ± 0.05 and 0.86 ± 0.07 eV were found in pristine and degraded states, respectively. This behavior might originate from a reduced electric field near the depletion region due to (1) partial annihilation of the positive space

charge (due to accumulation of V_O^{\bullet} by the negative interface charge created via trapped electrons at the Mn sites or/and (2) the shift in the center of charge into the bulk of the film due to the wide distribution of Mn ions throughout the film. In principle, a high concentration of V_O^{\bullet} , compensated via electrons, should exist near the cathode, which should lower the Schottky barrier. Failure to observe a change in Schottky barrier height upon electrical degradation suggests trapping of electrons and holes on Mn ions. Since the Mn ions are widely distributed within the film due to their low concentrations, the trapped electrons at Mn sites are also spread out, which prevents accumulation of electronic charges at the cathode/PZT film interface. This improves the resistance degradation behavior and lifetime of Mn doped PZT films.

Declaration of Competing Interest

The authors declare that they have no known competing financial interests or personal relationships that could have appeared to influence the work reported in this paper.

Acknowledgments

The authors gratefully acknowledge financial support from the Center for Dielectrics and Piezoelectrics and the National Science Foundation under grant nos. IIP-1361571 and IIP-1841453. The authors thank Minoru Ryu for TEM analysis.

Supplementary materials

Supplementary material associated with this article can be found, in the online version, at doi:10.1016/j.actamat.2021.116680.

References

- [1] R.G. Polcawich, M. Scanlon, J. Pulskamp, J. Clarkson, J. Conrad, D. Washington, R. Piekarz, S.E. Trolrier-McKinstry, M. Dubey, Design and fabrication of a lead zirconate titanate (PZT) thin film acoustic sensor, *Integr. Ferroelectr.* 54 (2003) 595–606.
- [2] Q. Zhou, S. Lau, D. Wu, K.K. Shung, Piezoelectric films for high frequency ultrasonic transducers in biomedical applications, *Prog. Mater. Sci.* 56 (2) (2011) 139–174.
- [3] Y. Qiu, J.V. Gigliotti, M. Wallace, M. F. Griggio, C.M.E. Demore, S. Cochran, S. Trolrier-McKinstry, Piezoelectric micromachined ultrasound transducer (PMUT) arrays for integrated sensing, actuation and imaging, *Sensors* 15 (2015) 8020–8041.
- [4] H.G. Yeo, X. Ma, C. Rahn, S. Trolrier-McKinstry, Efficient piezoelectric energy harvesters utilizing (001) textured bimorph PZT films on flexible metal foils, *Adv. Funct. Mater.* 26 (32) (2016) 5940–5946.
- [5] K. Morimoto, I. Kanno, K. Wasa, H. Kotera, High-efficiency piezoelectric energy harvesters of c-axis-oriented epitaxial PZT films transferred onto stainless steel cantilevers, *Sens. Actuators A* 163 (2010) 428–432.
- [6] H. Kueppers, T. Leuerer, U. Schnakenberg, W. Mokwa, M. Hoffmann, T. Schneller, U. Boettger, R. Waser, PZT thin films for piezoelectric microactuator applications, *Sens. Actuators A* 97 (2002) 680–684.
- [7] E. Defay, C. Millon, C. Malhaire, D. Barbier, PZT thin films integration for the realisation of a high sensitivity pressure microsensor based on a vibrating membrane, *Sens. Actuators A* 99 (2002) 64–67.
- [8] T. Kanda, T. Morita, M. Kurosawa, T. Higuchi, A rod-shaped vibro touch sensor using PZT thin film, in: *Proceedings of the IEEE Micro Electro Mechanical Systems (MEMS)*, 1998, pp. 378–383.
- [9] M.V. Raymond, D.M. Smyth, Defects and charge transport in perovskite ferroelectrics, *J. Phys. Chem. Solids* 57 (1996) 1507–1511.
- [10] N.R. Birkner, A. Navrotsky, Thermodynamic properties of manganese oxides, *J. Am. Ceram. Soc.* 79 (7) (1996) 1761–1768.
- [11] K. Hayashi, A. Ando, Y. Hamaji, Y. Sakabe, Study of the valence state of the manganese ions in PbTiO_3 ceramics by means of ESR, *Jpn. J. Appl. Phys.* 37 (1998) 5237–5240.
- [12] D. Hennings, H. Pomplun, Evaluation of lattice site and valence of Mn and Fe in polycrystalline PbTiO_3 by electron spin resonance and thermogravimetry, *J. Am. Ceram. Soc.* 57 (1974) 527–530.
- [13] B. Guiffard, E. Boucher, L. Eyraud, L. Lebrun, D. Guyomar, Influence of donor co-doping by niobium or fluorine on the conductivity of Mn doped and Mg doped PZT ceramics, *J. Eur. Cer. Soc.* 25 (2005) 2487–2490.
- [14] R.G. Polcawich, C-N Feng, S. Kurtz, S. Perini, P.J. Moses, S. Trolrier-McKinstry, AC and DC electrical stress reliability of piezoelectric lead zirconate titanate (PZT) thin films, *Intl. J. Microcircuits Elect Pack.* 23 (2000) 85–91.

- [15] P.F. Baude, C. Ye, D.L. Polla, Deep level transient spectroscopy characterization of ferroelectric Pb(Zr,Ti)O₃ thin films, *Appl. Phys. Lett.* 64 (1994) 2670–2672.
- [16] R-V Wang, P.C. McIntyre, ¹⁸O tracer diffusion in Pb(Zr,Ti)O₃ thin films: a probe of local oxygen vacancy concentration, *J. Appl. Phys.* 97 (2005) 023508-1-8.
- [17] H.N. Al-Shareef, D. Dimos, Leakage and reliability characteristics of lead zirconate titanate thin-film capacitors, *J. Am. Ceram. Soc.* 80 (80) (1997) 3127–3132.
- [18] J. Robertson, W.L. Warren, B.A. Tuttle, D. Dimos, D.M. Smyth, Shallow Pb³⁺ hole traps in lead zirconate titanate ferroelectrics, *Appl. Phys. Lett.* 63 (1993) 1519–1521.
- [19] S. Saremi S., R. Xu, L.R. Dedon, J.A. Mundy, S-L. Hsu, Z. Chen, A.R. Damodaran, S.P. Chapman, J.T. Evans, L.W. Martin, Enhanced electrical resistivity and properties via ion bombardment of ferroelectric thin films, *Adv. Mater.* 28 (2016) 10750–10756.
- [20] A. Peláiz-Barranco, J.D.S. Guerra, R. Lopez-Noda, E.B. Araujo, Ionized oxygen vacancy related electrical conductivity in (Pb_{1-x}La_x(Zr_{0.90}Ti_{0.10})_{1-x/4}O₃) ceramics, *J. Phys. D: Appl. Phys.* 41 (2008) 215503-1-5.
- [21] L. Andrejs, J. Fleig, Resistance degradation in donor-doped PZT ceramic stacks with Ag/Pd electrodes: I. Phenomenology of processes, *J. Eur. Ceram. Soc.* 33 (2013) 779–794.
- [22] B. Nagaraj, S. Aggarwal, T.K. Song, T. Sawhney, R. Ramesh, Leakage current mechanisms in lead-based thin-film ferroelectric capacitors, *Phys. Rev. B* 59 (1999) 16022–16027.
- [23] T-F. Zhang, X-G. Tang, Q-X. Liu, Y-P. Jiang, X-X. Huang, Oxygen-vacancy-related high temperature dielectric relaxation in (Pb_{1-x}Ba_x)ZrO₃ ceramics, *J. Am. Ceram. Soc.* 98 (2015) 551–558.
- [24] X. Wu, L. Liu, X. Li, Q. Zhang, B. Ren, D. Lin, X. Zhao, H. Luo, Y. Huang, Effect of annealing on defect and electrical properties of Mn doped Pb(Mg_{1/3}Nb_{2/3})O₃-0.28PbTiO₃ single crystals, *J. Cryst. Growth* 318 (2011) 865–869.
- [25] S. Zhao, S.J. Zhang, W. Liu, N.J. Donnelly, Z. Xu, C.A. Randall, Time dependent dc resistance degradation in lead-based perovskites: 0.7Pb(Mg_{1/3}Nb_{2/3})O₃-0.3PbTiO₃, *J. Appl. Phys.* 105 (2009) 053705-1-7.
- [26] C. Slouka, T. Kainz, E. Navickas, G. Walch, H. Hutter, K. Reichmann, J. Fleig, The effect of acceptor and donor doping on oxygen vacancy concentrations in lead zirconate titanate (PZT), *Materials* 9 (9) (2016) 945–967.
- [27] H. Ossmer, C. Slouka, L. Andrejs, P. Blaha, G. Friedbacher, J. Fleig, Electrocoloration of donor-doped lead zirconate titanate under DC field stress, *Solid State Ionics* 281 (2015) 49–59.
- [28] E. Bouyssou, P. Leduc, G. Guégan, R. Jérésian, Leakage current conduction in IrO₂/PZT/Pt structures, *J. Phys. Conf. Ser.* 10 (2005) 317–320.
- [29] G. Holzlechner, D. Kastner, C. Slouka, H. Hutter, J. Fleig, Oxygen vacancy redistribution in PbZr_xTi_{1-x}O₃ (PZT) under the influence of an electric field, *Solid State Ionics* 262 (2014) 625–629.
- [30] S-H. Yoon, C.A. Randall, K-H. Hur, Difference between resistance degradation of fixed valence acceptor (Mg) and variable valence acceptor (Mn)-doped BaTiO₃ ceramics, *J. Appl. Phys.* 108 (2010) 064101-1-9.
- [31] P.M. Raj, S. Xiang, M. Kumar M, I.R. Abothu, J-H. Hwang, Y. Liu, H. Yamamoto, R. Tummala, Leakage current suppression in solution-deposited barium titanate films on copper foils, *J. Mater. Sci.: Mater. Electron.* 23 (2012) 901–908.
- [32] T. Mori, K. Kakegawa, Improved reliability in thin-film capacitors fabricated with Mn-doped Pb(Zr,Ti)O₃ annealed at low temperatures, *Jpn. J. Appl. Phys.* 45 (2006) 7270–7274.
- [33] Y. Yan, K-H. Cho, S. Priya, Piezoelectric properties and temperature stability of Mn-doped Pb(Mg_{1/3}Nb_{2/3})-PbZrO₃-PbTiO₃ textured ceramics, *Appl. Phys. Lett.* 100 (2012) 132908-1-5.
- [34] B. Akkopru-Akgun, W. Zhu, M.T. Lanagan, S. Trolier-McKinstry, The effect of imprint on remanent piezoelectric properties and ferroelectric aging of Mn or Nb doped PbZr_{0.52}Ti_{0.48}O₃ thin films, *J. Am. Soc.* 102 (9) (2019) 5328–5341.
- [35] T.I. Prokopowicz, A.R. Vaskas, Research and Development Intrinsic Reliability Subminiature Ceramic Capacitors, 1969 Final Report Nos. ECOM-90705-F and NTIS AD-864068.
- [36] D.V. Lang, Deep-level transient spectroscopy: a new method to characterize traps in semiconductors, *J. Appl. Phys.* 45 (1974) 3023–3032.
- [37] T. Okamoto, T. J. Long, R.H.T. Wilke, J. Stitt, R. Maier, C.A. Randall, A charge-based deep level transient spectroscopy measurement system and characterization of a ZnO-based varistor and a Fe-doped SrTiO₃ dielectric, *Jap. J. Appl. Phys.* 55 (2016) 026601-1-6.
- [38] B. Ma, M. Narayanan, U.B. Balachandran, Dielectric strength and reliability of ferroelectric PLZT films deposited on nickel substrates, *Mater. Lett.* 63 (2009) 1353–1356.
- [39] W. Liu, C.A. Randall, Thermally stimulated relaxation in Fe-doped SrTiO₃ systems: II. Degradation of SrTiO₃ dielectrics, *J. Am. Ceram. Soc.* 91 (10) (2008) 3251–3257.
- [40] B. Akkopru-Akgun, D. Marincel, T. Bayer, K. Tsuji, C.A. Randall, M.T. Lanagan, S. Trolier-McKinstry, Thermally stimulated depolarization current measurements on degraded lead zirconate titanate films to be submitted to *J. Am. Ceram. Soc.*
- [41] B. Akkopru-Akgun, T. Bayer, K. Tsuji, C.A., Randall, M.T. Lanagan, S. Trolier-McKinstry, Leakage current characteristics and DC resistance degradation mechanisms in Nb doped PZT films to be submitted to *J. Appl. Phys.*
- [42] R-A. Eichel, Structural and dynamic properties of oxygen vacancies in perovskite oxides—analysis of defect chemistry by modern multi-frequency and pulsed EPR techniques, *Phys. Chem. Chem. Phys.* 13 (2011) 368–384.
- [43] J.F. Scott, K. Watanabe, A.J. Hartmann, R.N. Lamb, Device models for PZT/PT, BST/PT, SBT/PT, and SBT/BI ferroelectric memories, *Ferroelectrics* 225 (1999) 83–90.
- [44] A. Klein, Interface properties of dielectric oxides, *J. Am. Ceram. Soc.* 99 (2016) 369–387.
- [45] S. Takatani, K. Kushida-Abdelghafar, H. Miki, Effect of H₂ annealing on a Pb/PbZr_xTi_{1-x}O₃ interface studied by x-ray photoelectron spectroscopy, *Jpn. J. Appl. Phys.* 36 (1997) 435–438 36.
- [46] B. Jaffe, W.R. Cook, H. Jaffe, in: *Piezoelectric Ceramics*, Academic, London, 1971, pp. 237–245.
- [47] E.H. Rhoderick, R.H. Williams, in: *Metal-Semiconductor Contacts*, Clarendon, New York, 1988, pp. 284–295.
- [48] S.M. Sze, in: *Physics of Semiconductor Devices*, 2nd ed., Wiley, New York, 1981, pp. 52–58.
- [49] R.M. Waser, Dielectric analysis of integrated ceramic thin film capacitors, *Integr. Ferroelectr.* 15 (1997) 39–51.
- [50] B.A. Wechsler, M.B. Klein, Thermodynamic point defect model of barium titanate and application to the photorefractive effect, *J. Opt. Soc. Am. B- Opt. Phys.* 5 (1988) 1711–1723.
- [51] T.J.M. Bayer, J.J. Carter, J.-J. Wang, A. Klein, L-Q. Chen, C.A. Randall, Determination of electrical properties of degraded mixed ionic conductors: impedance studies with applied dc voltage, *J. Appl. Phys.* 122 (24) (2017) 244101-1-8..
- [52] T.J.M. Bayer, J.-J. Wang, J.J. Carter, L-Q. Chen, C.A. Randall, Impedance spectroscopy utilized to study the spatial distribution of conductivity within capacitors during operation, 2016 Jt. IEEE Int. Symp. Appl. Ferroelectr. Eur. Conf. Appl. Polar Dielectr., 1, 2016, doi:10.1109/ISAF.2016.7578078.
- [53] T.J.M. Bayer, J.-J. Wang, J.J. Carter, A. Moballeggh, J. Baker, D.L. Irving, E.C. Dickey, L-Q. Chen, The relation of electrical conductivity profiles and modulus data using the example of STO:Fe single crystals: a path to improve the model of resistance degradation, *Acta Mater.* 117 (2016) 252–261.
- [54] L.G. Escrig, M. Prades, H. Beltran, E. Cordoncillo, N. Maso, A.R. West, Voltage-dependent bulk resistivity of SrTiO₃: Mg ceramics, *J. Am. Ceram. Soc.* 97 (9) (2014) 2815–2824.
- [55] J. Dih, R.M. Fulrath, Electrical conductivity in lead zirconate-titanate ceramics, *J. Am. Ceram. Soc.* 61 (1978) 448–451.
- [56] D. Emin D., T. Holstein, Studies of small-polaron motion IV. Adiabatic theory of the Hall effect, *Ann. Phys.* 53 (1969) 439–520.
- [57] G.A. Samara, D. Emin, Pressure and temperature dependences of the electronic conductivity of boron carbides, *Phys. Rev. B* 32 (4) (1985) 2315–2318.